

Density of quasiparticle states for a two-dimensional disordered system: Metallic, insulating, and critical behavior in the class-D thermal quantum Hall effect

A. Mildenberger,^{1,2} F. Evers,^{2,3} A. D. Mirlin,^{2,3,*} and J. T. Chalker^{3,4}

¹*Fakultät für Physik, Universität Karlsruhe, 76128 Karlsruhe, Germany*

²*Institut für Nanotechnologie, Forschungszentrum Karlsruhe, 76021 Karlsruhe, Germany*

³*Institut für Theorie der Kondensierten Materie,
Universität Karlsruhe, 76128 Karlsruhe, Germany*

⁴*Theoretical Physics, University of Oxford, 1 Keble Road, Oxford OX1 3NP, UK*

(Dated: October 19, 2018)

We investigate numerically the quasiparticle density of states $\rho(E)$ for a two-dimensional, disordered superconductor in which both time-reversal and spin-rotation symmetry are broken. As a generic single-particle description of this class of systems (symmetry class D), we use the Cho-Fisher version of the network model. This has three phases: a thermal insulator, a thermal metal, and a quantized thermal Hall conductor. In the thermal metal, we find a logarithmic divergence in $\rho(E)$ as $E \rightarrow 0$, as predicted from sigma model calculations. Finite-size effects lead to superimposed oscillations, as expected from random matrix theory. In the thermal insulator and quantized thermal Hall conductor, we find that $\rho(E)$ is finite at $E = 0$. At the plateau transition between these phases, $\rho(E)$ decreases toward zero as $|E|$ is reduced, in line with the result $\rho(E) \sim |E| \ln(1/|E|)$ derived from calculations for Dirac fermions with random mass.

PACS numbers: 73.43.-f 73.20.Fz 74.78.-w

I. INTRODUCTION

The study of Anderson transitions – disorder-driven transitions in systems of noninteracting fermions – has a long history in condensed-matter physics. Symmetry is a guide to understanding both mesoscopic behavior in each phase and critical behavior at a transition. According to the symmetry classification inherited from random-matrix theory, in a conventional situation three Wigner-Dyson symmetry classes – orthogonal, unitary and symplectic – can be distinguished, depending on whether or not the Hamiltonian is invariant under time reversal and spin rotation (see Refs. 1,2,3,4,5 for reviews). Above a lower critical dimension, systems in each symmetry class can have a transition between insulating and metallic phases. In addition, in two-dimensional systems without symmetry under time-reversal or parity, a second type of insulating phase is possible, with edge states and a quantized Hall conductance, and there can be a plateau transition between the insulator and the quantized Hall conductor. Long-distance properties of these systems are described by nonlinear sigma models. Within this framework, quantized Hall conductors appear if symmetry allows a topological term in the sigma model.⁶

All Anderson transitions in the standard, Wigner-Dyson symmetry classes are expected to share certain general features. One is that the density of states (DoS) is a smooth function of energy, and hence noncritical at a transition. Another is universality, in the sense that, for a given symmetry and dimensionality, only one type of behavior is expected.

It is now widely appreciated that the range of possibilities is not exhausted by the Wigner-Dyson classes, and there exist additional symmetry classes. These additional classes are distinguished from the standard ones

by possessing a particle-hole symmetry that selects as special one particular energy E in the spectrum (we take this to be $E = 0$). Moreover, their density of states may be singular at $E = 0$ and may have distinct behavior in each phase and at a critical point. While individual examples of systems from the additional symmetry classes have been known for many years, as tight-binding models with two sublattice structure,^{7,8,9} within random-matrix theory,^{10,11} and as models for superconductors,¹² a full classification scheme was developed only more recently by Altland and Zirnbauer.^{13,14} This scheme includes, in addition to the Wigner-Dyson classes, systems belonging to two additional types of symmetry class. One set, the chiral classes, arises in two sublattice systems. The other set is realized in models for noninteracting quasiparticles in disordered superconductors based on Bogoliubov-de Gennes Hamiltonians. The properties of models belonging to these additional symmetry classes have been a focus of attention in connection with understanding low-energy quasiparticle DoS, transport, and localization properties in dirty superconductors, including those with unconventional pairing.^{13,15,16,17,18,19,20,21,22,23} Among other features, the additional symmetry classes allow for versions of the quantum Hall effect (QHE) in two-dimensional disordered superconductors with broken time-reversal symmetry. The relevant quantized conductance in these cases is a thermal or spin conductance, since quasiparticle number is not conserved by the Hamiltonian. For superconductors that are invariant under spin-rotations, the symmetry is referred to as class C, and the version of the quantum Hall effect is known as the spin QHE. Without spin rotation invariance, the symmetry is termed class D and one has the thermal QHE. The Hamiltonian for a system of the class D has the following block structure

in the particle-hole space¹³:

$$H = \begin{pmatrix} h & \Delta \\ -\Delta^* & -h^T \end{pmatrix}, \quad h = h^\dagger, \quad \Delta = -\Delta^T, \quad (1)$$

which is determined by the condition $H = -\sigma_x H^T \sigma_x$ (in addition to the Hermiticity $H = H^\dagger$). Alternatively, one can work in a different basis, defining $\tilde{H} = g^\dagger H g$ with $g^2 = \sigma_x$. In this basis, the defining condition of class D becomes $\tilde{H} = -\tilde{H}^T$, so that \tilde{H} is purely imaginary. It is the systems with this symmetry that are the subject of the present paper.

A striking feature of this class is that symmetry and dimensionality alone are insufficient to determine behavior. At the level of the nonlinear sigma model, the reason is believed to be that the relevant target space has two disconnected pieces and that, depending on the choice of underlying microscopic model, it may or may not be necessary to consider configurations containing domain walls on which the sigma model field jumps between the two components.^{21,24,25} In the following, we investigate the Cho-Fisher (CF) network model²⁶ for the thermal QHE. This model is generic in the sense that it displays all three phases possible in a two-dimensional class D system: the metal, the insulator, and the quantized Hall conductor. By contrast, in a closely related model – a fermionic version of the $\pm J$ random bond Ising model (RBIM) – the metallic phase is absent.²⁴

The location of the metallic phase and the two localized phases in the phase diagram of the CF model is indicated in Fig. 1, together with phase boundaries of two types, corresponding to metal-insulator and plateau transitions, respectively. This phase diagram was obtained in Ref. 23 from transfer-matrix calculations; let us explain why its structure may be quite naturally anticipated. In the absence of disorder ($p = 0$) the system has a gap around $E = 0$ for all α except for $\sin^2 \alpha = \frac{1}{2}$ (where the DoS vanishes linearly at zero energy). One thus expects that the system remains insulating for weak disorder (small p). More carefully, analyzing the edge states in the both limits of uncoupled plaquettes, $\sin^2 \alpha = 0$ and $\sin^2 \alpha = 1$, one observes that there are two topologically different insulating phases. From symmetry, if there is a direct transition between these phases, it must occur at $\sin^2 \alpha = \frac{1}{2}$. Finally, with increasing p , the disorder creates a substantial DoS at $E = 0$, and the system may be expected to undergo a transition into the metallic phase, which generically exists in two-dimensional systems with spin-orbit coupling.

Two-dimensional systems from class D have attracted considerable attention recently. The sigma model analysis^{16,21} starts from a short-distance description in terms of a diffusive metal with a smooth DoS that is finite at $E = 0$. From a renormalization group (RG) analysis (perturbative in g^{-1} , the inverse dimensionless conductance), it is found that the diffusion constant is unrenormalized at leading order and that the DoS has a logarithmic divergence near zero energy, which is given in terms of the diffusion constant D and the mean free

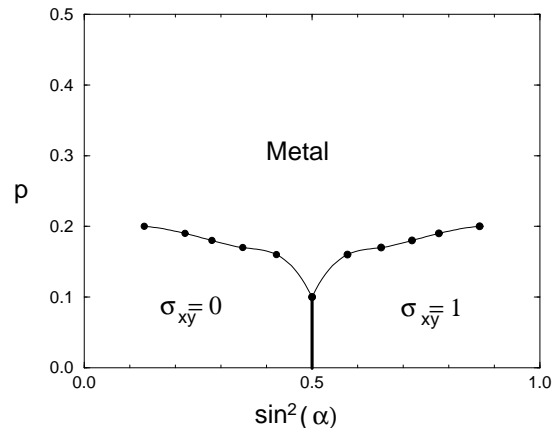


FIG. 1: Phase diagram of the Cho-Fisher model as obtained in Ref. 23 from transfer-matrix calculations. The plane is spanned by the parameters $\sin^2(\alpha)$, the interplaquette tunneling probability, and p , the concentration of vortex disorder: these control the short-distance values of the conductivity components σ_{xy} and σ_{xx} , respectively.

path ℓ_0 by

$$\varrho(E) = \varrho_0 + \frac{1}{4\pi^2 D} \ln \frac{D}{|E|\ell_0^2}. \quad (2)$$

An alternative approach to the theory of these systems, arguably tailored to describe the plateau transition, has been developed in Ref. 21 by starting from a model of Dirac fermions with random mass and treating this disorder perturbatively, in the spirit of the analysis of the Ising model by Dotsenko and Dotsenko.²⁷ The disorder-free system has a transition, driven by tuning a uniform mass through zero, which in the CF model lies at $p=0$, $\sin^2(\alpha)=1/2$. In the vicinity of the clean fixed point representing this transition, the disorder strength g_M is marginally irrelevant. This implies for the critical DoS a logarithmic correction term (see Appendix A) of the form

$$\varrho(E) = \frac{|E|}{2\pi} \left(1 + \frac{2g_M}{\pi} \ln \frac{1}{|E|} \right). \quad (3)$$

Clearly, since this calculation is for a system with weak, homogeneous disorder, its relevance for behavior in the CF model with dilute, strong scatterers needs to be tested.

In the localized phases, past work suggests several possibilities for the behavior of the DoS near $E=0$. The simplest approach is to imagine that the sample can be divided into independent regions of size set by the localization length and that the contribution of each region to the DoS can be obtained from random-matrix theory for this symmetry class,¹³ giving finite $\varrho(E)$ at $E=0$. Alternatives are suggested by the fact that the off-critical, disorder-free model ($p=0$, $\sin^2(\alpha) \neq 0$) has a gap in the

DoS around $E = 0$. As has been well-studied in one-dimensional system, rare disorder configurations (termed Griffiths strings) may fill in this gap, generating a DoS that varies as a positive or negative power of $|E|$ near $E=0$.^{17,18} Behavior of this kind has been found recently in the network model representation of the RBIM.²⁸

The purpose of this article is to present numerical studies of the behavior of the DoS in the CF model. An outline is as follows. In Sec. II, we describe the model and our numerical methods. Section III is central for the paper and contains our main findings. We analyze first (Sec. III A) the low-energy DoS in the metallic phase (at large p) and confirm the logarithmic divergence, Eq. (2). As an additional manifestation of metallic behavior, we find random-matrix-theory (RMT) oscillations in the DoS superseding this logarithmic behavior at lowest energies. At smaller p , one enters a localized phase (Sec. III B) where neither a logarithmic divergence nor oscillations are observed. Instead, the DoS remains finite at zero energy. Finally, in Sec. III C, we turn to the plateau transition which occurs for low p on the self-dual line $\sin^2(\alpha)=1/2$ (see Fig. 1). We find in a wide energy interval that the behavior of DoS is consistent with the RG result, Eq. (3). In Sec. IV we summarize our findings and discuss directions for future work. A brief description of an alternative microscopic model and results obtained for it are given in Appendix B: these results are very close to those for the CF model, supporting the idea that the latter is generic.

II. MODEL

The CF model²⁶ belongs to the family of network models first proposed in Ref. 29 for the description of the (conventional) quantum Hall effect. The structure of the network in the clean limit is shown in Fig. 2. The model describes quantum dynamics of noninteracting particles living on the directed links of a square network. If (as here) the wave function on a link has one component, the state of the system as a whole is represented by an N -component vector, where N is the number of links. The time evolution is characterized by a $N \times N$ unitary matrix \mathbf{U} , which in the absence of disorder is governed by a single parameter, $0 < \alpha < \pi/2$. At every node of the network the particle turns right or left with a probability amplitude $\pm \cos \alpha$ or $\pm \sin \alpha$, respectively. The amplitude signs are shown in Fig. 2 and ensure unitarity of the evolution operator \mathbf{U} .³⁰ Note that each plaquette of the network carries half a flux quantum so that particles pick up a phase factor π when moving around it.

In the absence of disorder, the parameter α is the same for all the nodes; then the network is a fermionic representation of the clean Ising model and \mathbf{U} can be diagonalized by Fourier transform. Near the critical point and for small wave vectors k , the spectrum has a Dirac form $E = (k^2 + \xi^{-2})^{1/2}$. The gap $\xi^{-1} = |\alpha - \pi/4|$ vanishes at the critical point $\alpha = \alpha_c \equiv \pi/4$ where the DoS is linear

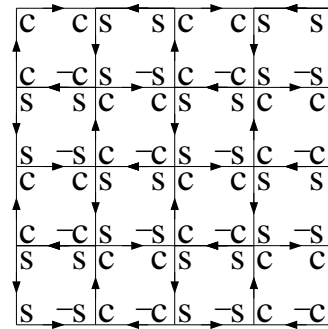


FIG. 2: Network representation of the clean Ising model. The plaquettes form two sublattices, C and S. The symbols “s” and “c” denotes the amplitudes for left and right turns, $\pm \sin \alpha$ and $\pm \cos \alpha$, governing the evolution at the network nodes. Adding disorder by inserting a vortex pair corresponds to flipping the signs of either a pair of s or a pair of c that are associated with a given node.

in energy: $\varrho(E) = |E|/2\pi$.

One can think of the evolution \mathbf{U} as being generated by a Hamiltonian. Taking $\mathbf{U} = \exp(-i\tilde{H})$, the symmetry condition for class D, that \tilde{H} is purely imaginary, implies that \mathbf{U} is real. Hence, within symmetry class D, disorder can be introduced into the model by allowing for node-to-node variation of the parameter α . This can be done in a variety of ways. A disorder weak in the perturbative sense of Refs. 27 and 21 can be realized by drawing α for every node from a distribution with a width $\delta\alpha$ that is small compared to the mean value. In contrast, in the CF model, disorder is introduced as isolated defects by making the change $\alpha \rightarrow -\alpha$ or $\alpha \rightarrow \pi - \alpha$, for a subset of nodes randomly distributed with a concentration p . This amounts to flipping signs of either both $\sin \alpha$ or both $\cos \alpha$ associated with such a node. This procedure can be viewed as the insertion of two additional half-flux lines into two plaquettes adjacent to the node and belonging to the same sublattice, see Fig. 2. Note that the vortex pair appears with equal probability on the C- or S-sublattice. It is this feature that distinguishes the CF model from the RBIM,^{26,31} which is obtained if all the additional vortices are placed on the same sublattice.

Our numerical analysis centers on the matrix \mathbf{U} for a system with a torus geometry of size $L \times L$. Since \mathbf{U} is unitary, its L^2 eigenvalues e^{iE_j} lie on the unit circle, defining the energies E_j . For a given realization of disorder, we compute eigenstates in a vicinity of the value $E=0$, where the special features of class D reveal themselves. For this purpose, we use efficient sparse matrix packages.^{32,33,34} The procedure is performed for an ensemble consisting typically of 10^4 or 10^5 disorder realizations, and the DoS is obtained as an ensemble average.

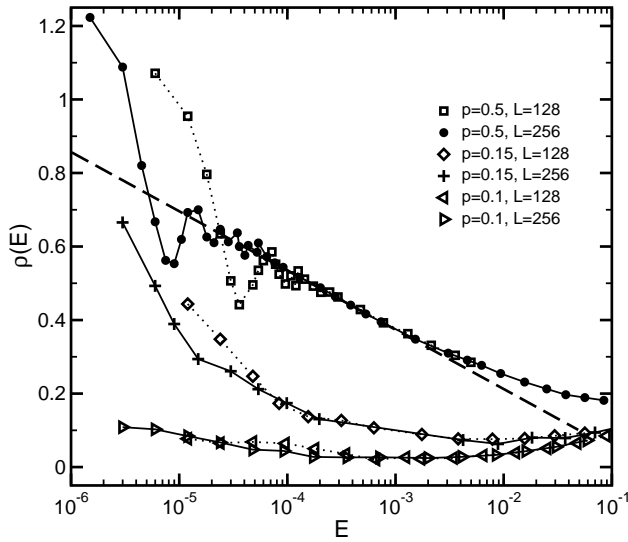


FIG. 3: Low-energy DoS in the metallic phase. Parameters (upper curves): $p=0.5$, $\alpha=\pi/4$, system sizes $L=128$ (squares), and $L=256$ (full circles). The straight dashed line represents the logarithmic asymptotics. For lowest energies, the RMT oscillations are clearly visible; they can be collapsed on a single curve, as shown in Fig. 4. For comparison, the results for $p=0.15$ and $p=0.1$ are also shown.

III. RESULTS AND DISCUSSION

A. Thermal metal

Before presenting our results for the metallic phase and comparing them to the analytical prediction Eq. (2), we briefly recall the theoretical framework within which Eq. (2) is obtained.^{16,21} Using the standard procedure, one derives an effective field theory that has the form of a diffusive supersymmetric nonlinear sigma model. This theory is valid on energy scales $E < \tau^{-1}$, where τ^{-1} is the elastic transport scattering rate. For the lowest energies, $E < E_{\text{Th}}$, below the Thouless energy E_{Th} (the inverse time of diffusion through the system), the theory becomes effectively zero-dimensional and reproduces the random-matrix theory of class D. A renormalization-group analysis, perturbative in the running coupling constant f (which is proportional to g^{-1}), yields

$$\frac{df}{d \ln \ell} = -f^2, \quad (4)$$

where ℓ denotes the ultraviolet cutoff. This implies that the infrared behavior of the system is governed by the perfect-metal fixed point, $f \rightarrow 0$. In other words, with increasing system size L , the conductance of the metal increases logarithmically, $g(L) \propto \ln L$, and hence diverges in the limit $L \rightarrow \infty$, so that the perturbative RG is justified. A similar analysis yields the RG equation for the second coupling constant ϵ , whose bare value is given by

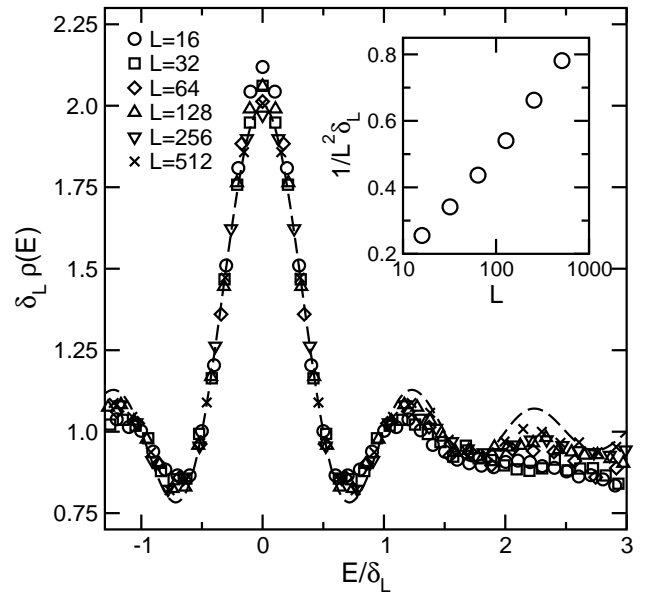


FIG. 4: Renormalized DoS at maximal disorder $p=0.5$ and on the symmetry line $\sin^2 \alpha=1/2$ for different system sizes vs the energy measured in units of the level spacing δ_L . The RMT result, Eq. (7), is plotted as a dashed line for comparison. The inset shows the logarithmic dependence of $1/L^2 \delta_L$ on the system size L , consistent with the data of Fig. 3. A fit of the slope yields $\varrho_0 f_0 = 0.152$ corresponding to $D = 0.33$.

the energy E ,

$$\frac{d\epsilon}{d \ln \ell} = (2 + f)\epsilon, \quad (5)$$

leading to Eq. (2) for the DoS. Comparing Eqs. (4) and (5), one sees that the logarithmic increase in the conductance is driven by the logarithmically divergent density of states, while the diffusion constant D remains nonsingular to this order.

We now turn to the results of our numerical simulations. Fig. 3 shows the DoS calculated at the maximal concentration p of flux lines, $p=1/2$. The data exhibit a logarithmic increase of the DoS over almost three decades in E for the larger system size, $L=256$. We stress that the increase continues to be of logarithmic form even though the renormalized DoS at small energies becomes much larger than its bare (large- E) value $\varrho_0 \simeq 0.1$. This is a signature of the fact that the RG flow is toward *weak coupling*, so that the one-loop result (2) is valid down to arbitrarily low energies in the thermodynamic limit.

At the smallest energies, we observe pronounced oscillations in the DoS. These are RMT oscillations due to finite system size and serve as another indication of the fact that we are dealing with a metallic phase. To demonstrate the RMT origin of these oscillations, we replot these parts of DoS curves, rescaling the energy to the mean level spacing δ_L at lowest energy for the corresponding system size. Specifically, δ_L is obtained by numerically solving $\varrho(\delta_L) = 1/L^2 \delta_L$ as suggested by Eq. (7) below. The results are shown in Fig. 4 for six different

system sizes. The data collapse on a single curve, which shows that the (renormalized) level spacing

$$\delta_L = \frac{1}{L^2 \varrho(E_{\text{Th}})} = \frac{1}{L^2 \varrho_0 [1 + f_0 \ln(L/\ell_0)]} \quad (6)$$

is indeed the only relevant energy scale in the regime $E \lesssim E_{\text{Th}}$ where the RMT is applicable. As further shown in Fig. 4, the curve obtained agrees nicely with the RMT prediction,

$$\varrho(E) = \frac{1}{L^2 \delta_L} \left[1 + \frac{\sin(2\pi E/\delta_L)}{2\pi E/\delta_L} \right], \quad (7)$$

up to $E/\delta_L \sim 1.5$ -2; for larger energies, the oscillations are strongly suppressed. This is fully consistent with the exponential vanishing of the RMT oscillations beyond the Thouless energy (see, e.g., Ref. 5). With increasing system size, the ratio E_{Th}/δ_L increases (though only logarithmically), so that the RMT range includes progressively more oscillation periods. This tendency is clearly seen in Fig. 4.

For comparison, we also show in Fig. 3 the low-energy DoS for $p = 0.15$ and $p = 0.1$; the latter point is close to the expected boundary of the metallic phase, see Fig. 1. It is seen that when the system approaches the phase boundary, the logarithmic increase of the DoS disappears and the RMT oscillations get damped.

B. Localized phases

Having explored the metallic phase, we now turn to the phases with localized states. Fixing the interplaquette coupling α at a value somewhat different from $\sin^2(\alpha)=1/2$ and decreasing the concentration p of vortex defects, we expect (see Fig. 1) that the system undergoes a transition at a critical value $p_c(\alpha)$ (which is of the order ~ 0.1) and enters the insulator or quantum Hall conductor. In both phases, bulk states are localized. Figure 5 demonstrates how this transition is reflected in the behavior of the DoS. In this figure, we display the evolution of the DoS at fixed tunneling probability $\sin^2 \alpha \simeq 0.58$ with decreasing defect concentration. The low-energy singular peak, whose magnitude increases logarithmically with the system size (as studied in Sec. III A), is still clearly seen for $p=0.13$ (see upper inset of Fig. 5) but is absent once p falls below 0.1 (lower inset of Fig. 5). Since this logarithmic singularity was a key signature of the thermal-metal phase, its absence signals the breakdown of the metallic behavior and, hence, the emergence of a localized phase.

For the localized phases, our main finding is that the DoS has a nonzero value at $E=0$. It is interesting to ask how this behavior connects with the value $\varrho(0)=0$ expected from Ref. 21 (see Eq. 3 above) at the plateau transition. Consider the DoS for α close to the critical value $\pi/4$, so that the localization length ξ is large. The behavior of DoS can then be understood by using

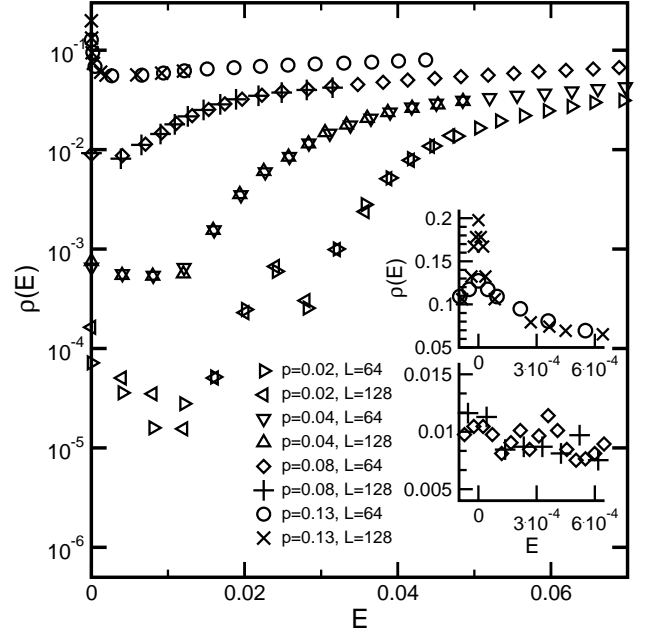


FIG. 5: DoS near $E = 0$ for disorder values $p = 0.13, 0.08, 0.04$, and 0.02 and for two system sizes $L = 64, 128$ at fixed interplaquette coupling $\sin^2(\alpha) = 0.579$. The DoS diverges logarithmically as $E \rightarrow 0$ in the metallic phase ($p = 0.13$) and remains finite in the localized phase (other values of p). The results for the lowest impurity concentration, $p = 0.02$, show an oscillatory feature induced by the band structure of the clean system, as well strong scatter in the data at the lowest energies, which is due to insufficient ensemble averaging. Upper inset: Low-energy peak at $p = 0.13$; its amplitude increases with L , in agreement with Sec. III A. Lower inset: Low-energy DoS at $p = 0.08$. No peak at $E \rightarrow 0$ is detected; $\rho(E \rightarrow 0)$ is a constant independent of L , indicating that the system is in the insulating phase. Statistical noise in the lower inset is more pronounced than in the upper one due to the smallness of the DoS.

the Dirac-fermion RG presented in Appendix A. Specifically, for energies that are not too small, behavior will be the same as at criticality, Eq. (3). However, for smallest energies, it is the localization length ξ (rather than E) that will terminate the RG process. In this sense, the role of ξ is fully analogous to that of finite system size L at criticality. This implies (see Appendix A) that $\varrho(E)$ saturates at the value

$$\varrho(E) \sim \frac{\ell_0}{\xi} \left(1 + 2 \frac{g_M}{\pi} \ln \frac{\xi}{\ell_0} \right)^{1/2}, \quad E \lesssim E_\xi, \quad (8)$$

where ℓ_0 is the ultraviolet cutoff length. The energy E_ξ at which the saturation takes place is

$$E_\xi \sim \frac{\ell_0}{\xi} \left(1 + 2 \frac{g_M}{\pi} \ln \frac{\xi}{\ell_0} \right)^{-1/2}. \quad (9)$$

The low-energy saturation of the DoS in the localized phases which we observe in our numerical simulations is fully consistent with these analytical predictions.

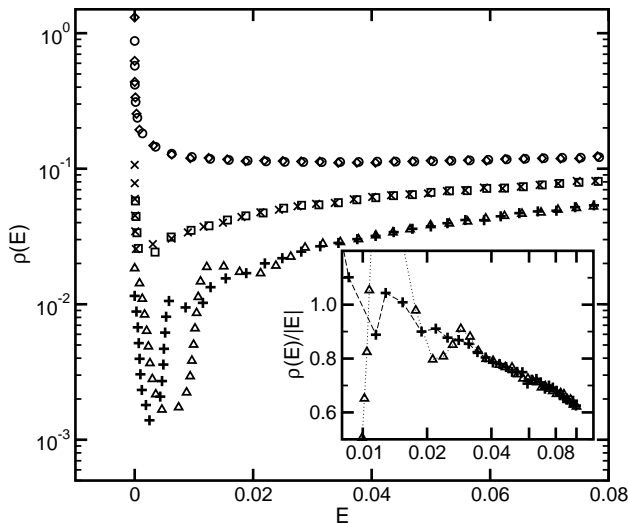


FIG. 6: DoS at low energy on the self-dual line $\sin^2(\alpha) = 0.5$ for disorder concentrations $p = 0.2$ (\circ, \diamond), 0.1 (\square, \times), and 0.05 ($\triangle, +$), where in each case, the first symbol is for $L = 128$ and the second is for $L = 256$. Inset: $\varrho(E)/|E|$ at $p=0.05$ on a log-linear scale. The logarithmic correction is clearly observed, in agreement with Eq. (3).

Before closing this subsection, we comment briefly on the regions of localized phases where the interplaquette coupling is very weak ($\sin^2 \alpha$ close to zero or to unity). As shown recently,²⁸ in this situation the DoS of the RBIM acquires a nonuniversal power-law singularity, $|E|^{1/z-1}$ with $z > 1$ associated with Griffiths strings.^{17,18} We expect that the same mechanism should be operative in the Cho-Fisher model as well. An analysis of these parts of the phase diagram and of the expected Griffiths singularities is, however, outside the scope of the present paper.

C. Plateau transition: $\sin^2 \alpha = 1/2$

The phase boundary between the insulator and thermal Hall conductor is the location of the plateau transition. From the treatment of Ref. 21 (see also Appendix A), RG flow on this boundary is toward the clean Ising fixed point. The corresponding RG result for the critical DoS is given by Eq. (3). To test this prediction, we have studied the evolution of the DoS on the self-dual line $\sin^2 \alpha = 1/2$ with decreasing concentration p of disorder. Results are shown in Fig. 6. For the largest two values, $p = 0.2$ and $p = 0.1$, the DoS exhibits a peak at $E = 0$ whose amplitude increases with L , which is a hallmark of the metallic phase (Sec. III B). For the lowest value, $p = 0.05$, this peak is not observed anymore, suggesting that this point belongs to the phase boundary between the two quantum Hall localized phases, see Fig. 1. Indeed, plotting $\varrho(E)/|E|$ as a function of $\log E$ (see the inset to Fig. 6), we find a behavior fully consistent with the logarithmic correction predicted by Eq. (3). At lowest energies, an oscillatory structure is observed in

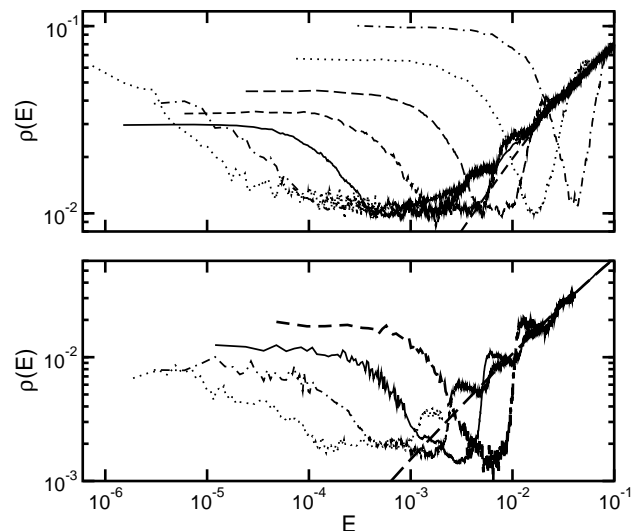


FIG. 7: Evolution of the DoS at low energies with increasing system size. DoS obtained by binning the 16 lowest-lying eigenvalues calculated for each network operator out of an ensemble of typically 10^4 disorder realizations. The step-like structures in the DoS is a remnant of the band structure of the clean lattice and their effect gradually diminishes with L increasing. Bold dashed lines show a fit to Eq. (3), $\varrho(E)/|E| = c_1 \ln |E_0/E|$. Upper panel: $p=0.08$, $L=16, 32, 64, 128, 256, 512, 1024$, $c_1=0.524$, $E_0=0.433$. The position of the sharp minimum occurring at small system sizes, $L=16, 32$, indicates the mean level spacing in these samples. Lower panel: $p=0.05$, $L=128, 256, 512, 1024$, $c_1=0.1875$, $E_0=2.865$.

the DoS curve for $p = 0.05$ in Fig. 6. This feature is a finite-size effect and is governed by the few lowest-lying eigenstates which inherit information on their position in the clean system. With increasing system size, the energy window for these oscillations shrinks, so that the DoS acquires a smooth limiting form in the thermodynamic limit.

We turn now to the analysis of the small- p DoS at asymptotically low energies. This requires investigation of system sizes larger than those used in Fig. 6. We show in Fig. 7 a log-log plot of the DoS for the disorder concentrations $p = 0.08$ and $p = 0.05$ (i.e., below the expected position of the three-critical fixed point, $p_T=0.1$, Fig. 1) and for system sizes up to $L = 1024$. It is seen that, when oscillations corresponding to the lowest discrete states are discarded, data for different L nicely combine in a single smooth curve corresponding to the thermodynamic-limit DoS. At moderately low energy, this curve is well fitted Eq. (3). So, up to this point, the behavior appears to be consistent with the expectation that the RG flow is directed toward the clean Ising fixed point. However, below $E \sim 10^{-2}$ ($E \sim 10^{-3}$) for $p=0.08$ ($p=0.05$), the DoS saturates. For $p=0.08$, it shows even an upturn for $E \lesssim 10^{-3}$; curves for $p=0.05$ suggest a similar tendency.

We do not have an unambiguous interpretation of these surprising findings and can only speculate about possible

scenarios.

(i) One possibility is that the position p_T of the tricritical point T is, in fact, not $p_T \simeq 0.1$ as was found in Ref. 23 (the phase diagram is reproduced in our Fig. 1) but rather considerably smaller, $p_T < 0.05$. In addition to a conflict with the data of Ref. 23, it would be quite surprising if such a numerically small value of p_T should arise. Also, it is pretty unexpected that after having reached the value of DoS as low as $\varrho \sim 10^{-3}$ (lower panel of Fig. 7), the system flows toward the metallic fixed point.

(ii) A more sophisticated scenario that would allow reconciliation of our results with those of Ref. 23 is that, in fact, there are two fixed points on the expected quantum Hall transition line $\sin^2 \alpha = 1/2$. Namely, in addition to the tricritical point p_T , there is a repulsive fixed point at some $p_N < p_T$. This point would then act as a “flow splitter” which is similar to the role of the Nishimori point in the RBIM (hence, the subscript N).

Taking this idea further, we could imagine that the tricritical point T also has a counterpart in the RBIM, namely, the zero-temperature transition point from the ferromagnetic phase into the spin glass. Furthermore, it is possible that the metallic phase of CF model connects to the spin-glass line of RBIM that exists at zero temperature for sufficiently strong disorder.

(iii) Another nontrivial possibility is that the RG treatment of the theory of Dirac fermions with Gaussian random mass is, in fact, insufficient, and some effects – possibly of nonperturbative origin – eventually drive the system away from the clean Ising fixed point.

In order to decide which of these scenarios take place, further work (analytical as well as numerical) is apparently needed. We will return to possible directions of future research in Sec. IV.

IV. CONCLUSIONS

In summary, we have presented a numerical investigation of the density of states $\varrho(E)$ in the Cho-Fisher network model. The model is a generic two-dimensional representative of the symmetry class D describing disordered superconductors with broken spin-rotation and time-reversal invariances, and shows the thermal quantum Hall effect. At a sufficiently large concentration p of defects, the DoS has a logarithmic divergence as $E \rightarrow 0$ with superimposed random-matrix-theory oscillations, in agreement with analytical predictions for the thermal-metal phase, given in Eqs. (2) and (7). Reducing p , we find a transition into localized phases (insulator and quantized Hall conductor) with $\varrho(E)$ finite at $E=0$.

At the plateau transition between these phases, the DoS tends to vanish as $E \rightarrow 0$ in agreement with the behavior $\varrho(E) \sim |E| \ln(1/|E|)$ derived from the theory for Dirac fermions with random mass, Eq. (3). However, at lowest E , this behavior breaks down, and DoS saturates and even shows an upturn. We do not have an unambigu-

ous explanation for this behavior; more work is needed in order to understand better the properties of the system at the quantum Hall transition line. We imagine an analysis of a phase diagram of a wider family of class-D models, see Ref. 35. One can also study the dependence of results on the microscopic model in numerical simulations. In particular, a possible generalization of the Cho-Fisher model is presented in Appendix B. Further, one should study different observables that are more susceptible to the critical behavior and would give additional information about the system at the expected critical line. In particular, an analysis of the wave-function statistics is expected to be useful in this respect.³⁶

Acknowledgments

We thank I. A. Gruzberg, V. Kagalovsky, A. W. W. Ludwig, R. Narayanan, X. Wan, and M. R. Zirnbauer for fruitful discussions. This work was supported by the SPP “Quanten-Hall-Systeme” and Center for Functional Nanostructures of the DFG and by the A. von Humboldt Foundation.

APPENDIX A: RENORMALIZATION GROUP FOR DIRAC FERMIONS WITH RANDOM MASS

In this Appendix, we sketch the RG analysis of the DoS of Dirac fermions with random mass, leading to Eq. (3) at criticality and Eq. (8) away from the critical line. Our presentation largely follows Ref. 21 though we depart from that work at the end. The Hamiltonian has the form

$$H = -i\partial_x \sigma_x - i\partial_y \sigma_y + m(\mathbf{r})\sigma_z, \quad (\text{A1})$$

where σ_μ are Pauli matrices. It satisfies the Hermiticity $H = H^\dagger$ and the class-D symmetry, $H = -\sigma_x H^T \sigma_x$. The mass $m(\mathbf{r})$ is a Gaussian random variable, with

$$\langle m(\mathbf{r})m(\mathbf{r}') \rangle = 2g_M \delta(\mathbf{r} - \mathbf{r}'). \quad (\text{A2})$$

Introducing the field-theoretical representation, performing the disorder averaging, and carrying out the RG analysis (see Ref. 21), one gets in one-loop order the scaling equations for renormalization of the disorder strength g_M and the energy E ,

$$\frac{dg_M}{d \ln \ell} = -\frac{2g_M^2}{\pi}; \quad (\text{A3})$$

$$\frac{dE}{d \ln \ell} = \left(1 + \frac{g_M}{\pi}\right) E. \quad (\text{A4})$$

Here, ℓ is the ultraviolet cutoff. The model is originally defined with a microscopic cutoff ℓ_0 (lattice spacing), so that $E \equiv E(\ell_0)$ and $g_M \equiv g_M(\ell_0)$. Our aim is to analyze the DoS, $\varrho(E) \equiv \varrho(E(\ell_0), g_M(\ell_0), \ell_0)$. Integrating these

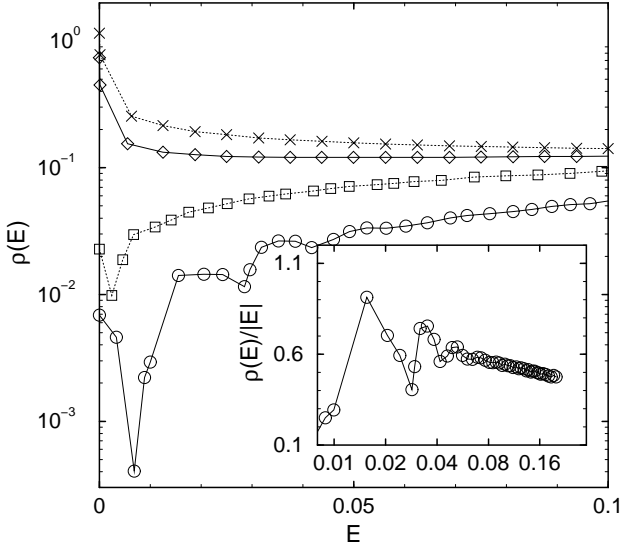


FIG. 8: DoS near $E = 0$ on the self-dual line $\alpha_0 = \pi/4$ for the CDM with plaquette coupling parameter α continuously distributed within the window $\Delta\alpha$. Evolution from metallic to critical behavior is clearly observed with decreasing disorder strength. The four data curves (from top to bottom) are for $\Delta\alpha = 1.0$ (x), 0.8 (\diamond), 0.6 (\square), and 0.4 (\circ) with system size $L=128$. Inset: $\rho(E)/|E|$ on the log-linear scale (see inset of Fig. 6).

equations, one gets

$$g_M^{-1}(\ell) = g_M^{-1}(\ell_0) + \frac{2}{\pi} \ln \frac{\ell}{\ell_0}, \quad (\text{A5})$$

$$E(\ell) = E(\ell_0) \frac{\ell}{\ell_0} \left[1 + \frac{2g_M(\ell_0)}{\pi} \ln \frac{\ell}{\ell_0} \right]^{1/2}, \quad (\text{A6})$$

yielding

$$\rho(E(\ell), g_M(\ell), \ell) = \rho(E(\ell_0), g_M(\ell_0), \ell_0) \times \frac{\ell}{\ell_0} \left[1 + \frac{2g_M(\ell_0)}{\pi} \ln \frac{\ell}{\ell_0} \right]^{-1/2}. \quad (\text{A7})$$

There are two ways in which the renormalization can terminate: (i) $E(\ell)$ reaches the bandwidth (~ 1) or (ii) ℓ reaches the system size L . In the first case we use the fact that for large $E(\ell)$ the DoS is essentially unaffected by disorder, $\rho(E(\ell)) \simeq |E(\ell)|/2\pi$, yielding Eq. (3) of the main text for $|E| \gg E_0$, where E_0 is given by Eq. (A9). In the second case, we get after renormalization a system with just few degrees of freedom (ultraviolet cutoff of the order of the system size L) and a small energy $E(L) \ll 1$. Since the DoS is finite at $E=0$ in the random-matrix theory of class D, we find that

$$\rho(E) \sim \frac{\ell_0}{L} \left[1 + 2 \frac{g_M}{\pi} \ln \frac{L}{\ell_0} \right]^{1/2}, \quad E \ll E_0. \quad (\text{A8})$$

Comparing Eqs. (3) and (A9), we find that the energy E_0 at which the behavior (3) saturates in a finite system,

crossing over into Eq. (A8), is

$$E_0 \sim \frac{\ell_0}{L} \left[1 + 2 \frac{g_M}{\pi} \ln \frac{L}{\ell_0} \right]^{-1/2}. \quad (\text{A9})$$

Up to now, we considered a system exactly at criticality ($\alpha = \pi/4$ in the network model). Moving slightly off criticality, we enter the localized phase, with a localization length $\xi < \infty$. Since the states in different localization volumes are essentially independent, the localization length will play the same role as the system size L in Eqs. (3) and (A9). Substituting ξ for L , we obtain Eqs. (8) and (9) of the main text.

APPENDIX B: CONTINUOUS-DISORDER MODEL

The CF model can be defined as a network model with the following distribution of plaquette couplings:

$$\mathcal{P}(\alpha) = (1-p)\delta(\alpha - \alpha_0) + \frac{p}{2}\delta(\alpha + \alpha_0) + \frac{p}{2}\delta(\alpha + \alpha_0 - \pi). \quad (\text{B1})$$

It is natural to expect that properties will be qualitatively the same for any model with a *generic* distribution $\mathcal{P}(\alpha)$. A precise definition of the word “generic” is far from trivial in the present case. In particular, we know that the distribution

$$\mathcal{P}(\alpha) = (1-p)\delta(\alpha - \alpha_0) + p\delta(\alpha + \alpha_0) \quad (\text{B2})$$

corresponds to RBIM which does not possess a metallic phase and thus is not generic.

In order to test the expectation of (restricted) universality, we define a continuous-disorder model (CDM), with a Gaussian distribution for the angle α . The center α_0 of the distribution determines the breaking of the symmetry between the C and S plaquettes and thus governs the plateau transition. The width $\Delta\alpha$ determines the strength of disorder and therefore replaces the parameter p of the Cho-Fisher model.

In Fig. 8, we show the evolution of DoS on the self-dual line, $\alpha_0 = \pi/4$, with disorder strength decreasing from $\Delta\alpha = 1.0$ to 0.4 . We see that the behavior is very similar to that in the Cho-Fisher model, Fig. 6: we observe a transition from a metal (divergent DoS) to the critical region. Furthermore, the families of the curves look essentially identical in both cases. We interpret this as a confirmation of the generic character of the Cho-Fisher model.

We have not studied the behavior of DoS at weak disorder for lowest energies (where we observed a surprising upturn in the case of Cho-Fisher model), relegating a detailed investigation of this problem to future work,³⁶ where not only spectral properties but also those of wave functions will be analyzed.

-
- * Also at Petersburg Nuclear Physics Institute, 188300 St. Petersburg, Russia.
- ¹ P.A. Lee and T.V. Ramakrishnan, *Rev. Mod. Phys.* **57**, 287 (1985).
 - ² B. Kramer and A. MacKinnon, *Rep. Prog. Phys.* **56**, 1469 (1993).
 - ³ T. Guhr, A. Müller-Groeling, and H.A. Weidenmüller, *Phys. Rep.* **299**, 189 (1998).
 - ⁴ K.B. Efetov, *Supersymmetry in Disorder and Chaos* (Cambridge University Press, 1997).
 - ⁵ A.D. Mirlin, *Phys. Rep.* **326**, 259 (2000).
 - ⁶ B. Huckestein, *Rev. Mod. Phys.* **67**, 357 (1995).
 - ⁷ F. J. Dyson, *J. Math. Phys.* **3**, 140 (1962); **3**, 1199 (1962).
 - ⁸ T. P. Eggarter and R. Riedinger, *Phys. Rev. B* **18**, 569 (1978).
 - ⁹ R. Gade and F. Wegner, *Nucl. Phys. B* **360**, 213, (1991), R. Gade, *Nucl. Phys. B* **398**, 499, (1993).
 - ¹⁰ K. Slevin and T. Nagao, *Phys. Rev. Lett.* **70**, 635 (1993).
 - ¹¹ J. J. M. Verbaarschot and I Zahed, *Phys. Rev. Lett.* **70**, 3852 (1993).
 - ¹² R. Oppermann, *Physica A* **167**, 301 (1990).
 - ¹³ A. Altland and M.R. Zirnbauer, *Phys. Rev. B* **55**, 1142 (1997).
 - ¹⁴ M.R. Zirnbauer, *J. Math. Phys.* **37**, 4986 (1996).
 - ¹⁵ T. Senthil and M.P.A. Fisher, *Phys. Rev. B* **60**, 6893 (1999); S. Vishveshwara, T. Senthil and M.P.A. Fisher, *Phys. Rev. B* **61**, 6966 (2000); S. Vishveshwara and M.P.A. Fisher, *Phys. Rev. B* **64**, 174511 (2001).
 - ¹⁶ T. Senthil and M.P.A. Fisher, *Phys. Rev. B* **60**, 6893 (1999).
 - ¹⁷ O. Motrunich, K. Damle, and D. A. Huse, *Phys. Rev. B* **63**, 224204 (2001).
 - ¹⁸ O. Motrunich, K. Damle, and D. A. Huse, *Phys. Rev. B* **65**, 064206 (2002).
 - ¹⁹ P.J. Hirschfeld and W.A. Athkinson, *J. Low Temp. Phys.* **126**, 881 (2002).
 - ²⁰ A. Altland, B.D. Simons, and M.R. Zirnbauer, *Phys. Rep.* **359**, 283 (2002).
 - ²¹ M. Bocquet, D. Serban, and M. R. Zirnbauer, *Nucl. Phys. B* **578**, 628 (2000).
 - ²² V. Kagalovsky, B. Horovitz, Y. Avishai, and J.T. Chalker, *Phys. Rev. Lett.* **82**, 3516 (1999).
 - ²³ J. T. Chalker, N. Read, V. Kagalovsky, B. Horovitz, Y. Avishai, and A. W. W. Ludwig, *Phys. Rev. B* **65**, 012506 (2002).
 - ²⁴ N. Read and A.W.W. Ludwig, *Phys. Rev. B* **63**, 024404 (2001).
 - ²⁵ I. A. Gruzberg, N. Read, and S. Vishveshwara, *Phys. Rev. B* **71**, 245124 (2005).
 - ²⁶ S. Cho and M.P.A. Fisher, *Phys. Rev. B* **55**, 1025 (1997).
 - ²⁷ V.S. Dotsenko and V.I.S. Dotsenko, *Adv. Phys.* **32**, 129 (1983).
 - ²⁸ A. Mildenberger, F. Evers, R. Narayanan, A.D. Mirlin, and K. Damle, *Phys. Rev. B* **73**, 121301(R) (2006).
 - ²⁹ J.T. Chalker and P.D. Coddington, *J. Phys. C* **21**, 2665 (1988).
 - ³⁰ R. Klesse and M. Metzler, *Europhys. Lett.* **32**, 229 (1995).
 - ³¹ F. Merz and J. T. Chalker, *Phys. Rev. B* **65**, 054425 (2002).
 - ³² P.R. Amestoy, I.S. Duff, and J.-Y. L'Excellent, *Comput. Methods in Appl. Mech. Eng.* **184**, 501 (2000); P.R. Amestoy, I.S. Duff, J. Koster, and J.-Y. L'Excellent, *SIAM J. Matrix Anal. Appl.* **23**, 15 (2001).
 - ³³ J.W. Demmel, S.C. Eisenstat, J.R. Gilbert, X.S. Li, and J.W.H. Liu, *SIAM J. Matrix Anal. Appl.* **20**, 720 (1999).
 - ³⁴ R.B. Lehoucq, D. Sorensen, and C. Yang, *ARPACK Users Guide* (SIAM, Philadelphia, PA 1998).
 - ³⁵ I. A. Gruzberg, N. Read, and A. W. W. Ludwig, *Phys. Rev. B* **63**, 104422 (2001).
 - ³⁶ A. Mildenberger *et al.*, unpublished.